9-11-2013 12:00 AM

Investigating the Influence of Interface and Vacancy Defects on the Growth of Silicon Quantum Dots in SiO2

John Phelan
The University of Western Ontario

Supervisor
Dr. Peter Simpson
The University of Western Ontario

Graduate Program in Physics
A thesis submitted in partial fulfillment of the requirements for the degree in Master of Science

Recommended Citation

Phelan, John, "Investigating the Influence of Interface and Vacancy Defects on the Growth of Silicon Quantum Dots in SiO2" (2013). *Electronic Thesis and Dissertation Repository*. 1669.
https://ir.lib.uwo.ca/etd/1669

INVESTIGATING THE INFLUENCE OF INTERFACE AND VACANCY DEFECTS ON THE GROWTH OF SILICON QUANTUM DOTS IN SiO_2

(Thesis format: Monograph)

by

John Phelan

Graduate Program in Physics

A thesis submitted in partial fulfillment
of the requirements for the degree of
Master of Science

The School of Graduate and Postdoctoral Studies
The University of Western Ontario
London, Ontario, Canada

Abstract

The effects of interface and vacancy defects on silicon quantum dot (Si-QD) growth are investigated using measurements of Time Resolved Photoluminescence (TRPL), Photoluminescence (PL) Spectroscopy and Electron Paramagnetic Resonance (EPR). Thermally grown SiO_2 thin films (280nm) were irradiated with high energy (400keV – 1MeV) silicon ions in order to introduce defects into the Si-QD growth layer of SiO_2. A noticeable increase in PL emission intensity is seen with the highest energy pre-implanted sample over a single implant sample. TRPL results show increased radiative lifetimes for the lower energy (400keV) pre-implant while little or no difference is seen in TRPL results between the single implant and the higher energy implanted samples. The origin of increased PL emission intensity and a trend towards shorter radiative lifetimes with increased implant energy in TRPL measurements are believed to be due to defect-mediated Si-QD growth in high energy pre-implanted samples.

Keywords

Photoluminescence, silicon quantum dots, time resolved photoluminescence, Electron Paramagnetic Resonance.

Acknowledgments

I'd like to thank Dr. Peter Simpson, Dr. Lyudmila Goncharova, Sergey Dedulin, Dr. Eric Barbagiovanni, Dr. Giovanni Fanchini, Arash Akbari-Sharbaf and Dr. Patrick Wilson for their continued support and advice throughout my time at UWO.

Table of Contents

List of Figures

Chapter 1

1 Silicon Quantum dots and Nanophotonics

Photonics is a popular area of research for applications in computing, information processing and renewable energy technologies. The use of light for relaying information with minimal losses over long distances has existed for thousands of years, a classic example being the use of the Aldis Lamp as a reliable wireless communications device for more than a century.

Although technology has come a long way in a relatively short period, we still use light signals to relay information in fiber optic networks to interconnect electronic networks around the world. One major challenge is miniaturization of photonic systems so that light can be used not just in bulky interconnects between major networks but as an integral part of device technologies we rely on and use on a daily basis. While fiber optics is the backbone of the global information network, nanophotonics has the potential to revolutionize our communications networks by taking the place of electronics in interconnections and switches in data centers where systems run at very high capacities. Far from electronics in every day devices becoming obsolete, developments in nanophotonics for use in information bottlenecks can allow electronic communications to realize their full potential. Excess heat in traditional electronics systems not only inhibits performance but results in high energy consumption. Cooling is needed to maintain optimal (or even minimal) performance. One only has to look at heat generated by the microprocessor in a consumer laptop, which needs to be constantly cooled to prevent system meltdown. It isn't an overstatement to say that possibly the most important part of any computing system is cooling, without which the device would fail. Advancements in nanophotonics and their application in everyday life could address many of these issues leading to “greener”, more reliable and better performing information technologies and renewable energy systems.

Si-QD and SiO_2 luminescence is an area of much interest in nanophotonics. Si-QDs in SiO_2 can be fabricated by ion implantation (Iwayama 1994) and has been the subject of much research in the area of nanophotonics in the past two decades since the discovery of PL from porous silicon in 1990 (Canham 1990). Many novel photonic and optoelectronic devices such as solid state lighting (Humphreys 2008), optical chips (Graydon 2007) and solar cell technologies (Liu 2010) have already been developed with broad spectrum solid state lighting on consumer shelves already. Biological labeling (Zhao 2010) and non-volatile memory devices (Cy 2007) are also possible applications being investigated. In order for these devices to be developed for the market there is a need for tunable light sources (Zhizhong 2009) manufactured using techniques compatible with contemporary industrial methods. During the “Silicon Age” (Kittler 2006) many industrial processing techniques involving ion implantation into silicon have been developed. Its use as a basis for new technologies such as some of those mentioned above takes advantage of this fact. The synthesis of luminescent Si-QDs in SiO_2 is compatible with current industrial processes such as thin film growth via thermal oxidation, ion implantation and crystal growth by rapid thermal annealing.

1.1 Photoluminescence

In this work we are investigating the mechanisms behind photoluminescence (Dippo 2001) in Si-QD/SiO_2 thin films. Si-QD photoluminescence (PL) and electroluminescence (EL) (Pankove 1977) can be studied at room temperature which makes the experimental process more convenient.

Semiconductor PL is the emission of a photon through radiative relaxation after the absorption of light of high enough energy to cause interband electronic transitions. An interband electronic transition is the promotion of an electron from the valence band to the conduction band through the absorption of energy by the atoms in a material. Initially the atoms in a photoluminescent material are not in an excited state, that is, there are an equal number of holes in the valence band and electrons in the conduction band. In order to undergo interband transitions and be promoted from the valence band to the conduction band an electron must absorb a photon with energy corresponding, at a minimum, to the bandgap energy of that material. The bandgap of a material is the energy difference between the highest energy of the valence band and lowest energy of the conduction band.

Conservation of energy implies that the frequency (v) of the incoming photon must satisfy Eq.1 to impart enough energy for excitation.

$$E = hv = E_2 - E_1 \tag{1}$$

where E is the energy of the incoming photon, h is the Planck constant, E_1 is the highest energy level of the valence band and E_2 is the lowest energy level of the conduction band.

Once promoted to the conduction band an electron will spontaneously lose its excess energy and relax back down to the valence band and at the same time emit a photon. The relaxation process involves energy emitted as photons or energy dissipated as vibrations in the surrounding material. The time scale of competing radiative and non-radiative processes will influence their probability of occurrence and therefore the emission efficiency of the material in question. If non radiative processes occur on a shorter time scale than radiative processes then a material will emit little or no light. The frequency of the emitted photon during de-excitation will correspond to the energy bandgap (E_g) of the material.

1.1.1 Radiative Relaxation

Radiative relaxation occurs when an electron in a semiconductor material decays or relaxes back down to the valence band from the conduction band with the emission of a photon. The photon emitted will have a wavelength related to the energy difference between the conduction band and the valence band of the material as mentioned in the previous section and illustrated in Figure 1 in the case of a direct transition. For larger bandgap transitions the emitted light will be blue shifted and smaller bandgap transitions will be red shifted.

1.1.2 Direct and Indirect Bandgap Semiconductors

In a direct bandgap semiconductor or an indirect bandgap material where the transition rules are relaxed, electron decay from the conduction band to the valence band can result in the emission of a photon.

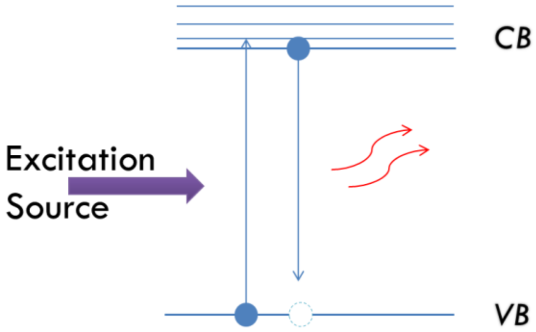

Figure 1: Photoluminescence due to absorption of light by an electron and subsequent radiative relaxation during the transition between the conduction band (CB) and valance band (VB).

The emission photon will have a wavelength corresponding to the energy gap of the material in question as is demonstrated in the operation of a Light Emitting Diode (LED). The color of a LED is a result of photonic emission from semiconductor material corresponding to the bandgap energy of that material. Silicon is an indirect bandgap semiconductor meaning that exciton generation or the transition of an electron from the valence band to the conduction band (excitation) is a two-step process. This is due to the fact that the lowest energy level of the conduction band is not at the Brillouin zone center so that it isn't directly in line in with the highest energy level of the valence band. An incoming photon imparts energy but not sufficient momentum to the system for excitation to occur, so the absorption of both a photon and a phonon must occur at the same time to ensure that energy and momentum are conserved and promotion of an electron to the conduction band occurs (Streetman 1997). Under normal circumstances this is very unlikely to occur in an indirect bandgap material given the offset band structure. This effect is also apparent during relaxation of an electron from conduction band to valence band of an indirect bandgap material where a phonon is needed. In an indirect bandgap semiconductor such as silicon a phonon must add momentum to the system at the same time as a photon is absorbed by an electron for transition of an electron from the valence band to the conduction band. Relaxation or electron-hole recombination is far less likely to be radiative resulting in emission of a photon. Non-radiative recombination is dominant resulting in energy emitted as vibrations, dissipating into the surrounding material without photoemission. In the case of Si-QD in SiO_2 the rules preventing radiative recombination are relaxed. This is due to electron confinement playing a role in the recombination mechanism. An exciton exists as a coupling of an electron in the conduction band and a “hole” in the valence band due to their Coulomb attraction. This bound state results in the pair revolving around their center of mass separated at a distance equal to that of the exciton Bohr radius. The Bohr radius is the most probable distance between the hydrogen proton and electron given by the Eq. 2,

$$a_H = \frac{4\pi\varepsilon_0\hbar^2}{m_e e^2} \tag{2}$$

where ε_0 is the permittivity of free space, $\hbar$ is the reduced Planck’s constant, m_e is the electron rest mass and e is the elementary charge. The exciton Bohr radius is found by applying the Bohr model to a free exciton as shown in Eq. 3,

$$a_{ex} = \frac{m_0\varepsilon_r}{\mu} \tag{3}$$

where m_0 is the mass of an electron, ε_r is the dielectric constant and μ is the reduced mass of the exciton. Using this equation the exciton Bohr radius of silicon is found to be 4.3nm in bulk crystalline silicon. In Si-QD with a radius approaching the exciton Bohr radius, a widening of the energy bands occurs which is explained in Section 1.2.

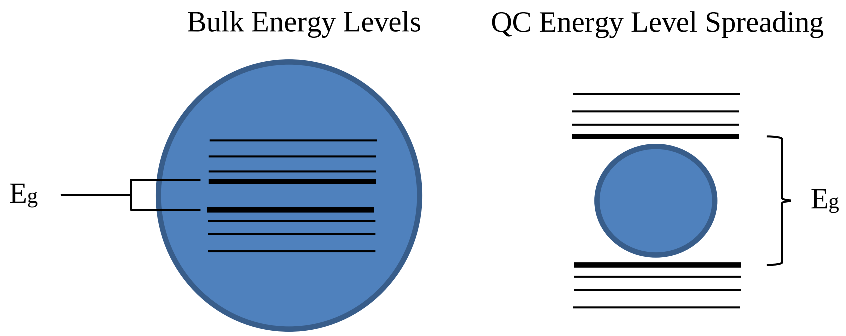

Figure 2: Bulk-scale vs nano-scale showing energy level broadening due to QC effects

This widening of energy bands increases the electron-hole separation, reducing the probability of non-radiative recombination allowing for the main recombination route to be radiative resulting in photo emission (Kovalev 1998). There exists an inverse relationship between Si-QD diameter and photon emission energy, as diameter decreases, energy of photons emitted increases as does their frequency. There is some evidence that smaller radius quantum dots can transfer excitation to larger quantum dots in clusters acting as donors with emission coming from the larger quantum dots (Jayatilleka 2011).

1.1.3 Excitons

Photon absorption followed by the promotion of an electron to an excited state leaves a net positive charge in the valence band due to the lack of negative charge from the electron. This net positive charge is referred to as a hole. Similarly the electron carries a net negative charge to the conduction band. If the electron-hole binding energy is greater than k_BT where k_B is the Boltzmann constant, then an exciton will form, separated by a_{ex} and attracted due to the Coulomb force. The lifetime of the exciton depends on whether its binding energy is strong enough to prevent it from coming into contact with phonons. Fewer defects result in a longer lifetime. In semiconductors, excitons exist as bound electron-hole pairs with separation distances of more than one lattice constant.

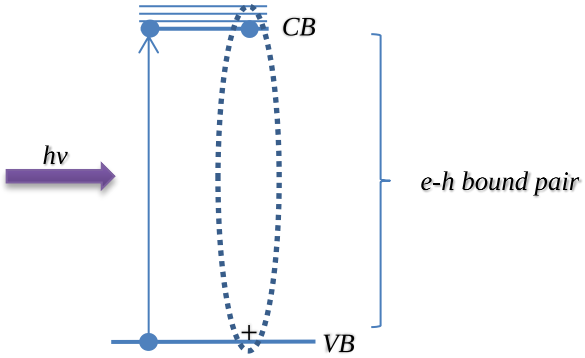

Figure 3: Electron-hole bound pair. This bound state can exist until such time as radiative or non-radiative relaxation occurs.

Since there is interaction between the electron and hole and they act as a bound pair or exciton, they are not seen as separate but as one quasiparticle for the lifetime of the exciton. Excitons occurring in semiconductors are known as Wannier excitons and often result in radiative recombination. Wannier excitons can be considered as similar to the hydrogen atom with one negative charge orbiting a positive charge. Adjusting the model of the hydrogen atom with a Bohr radius of 0.05nm, the exciton Bohr radius in a semiconductor can be calculated to be around 4.3nm. The weaker interaction as compared to the Bohr model is due to the larger radius of the Wannier exciton. In the hydrogen atom the electron is more tightly bound due to the larger relative mass of the proton resulting in increased Coulomb force interaction and a smaller radius. Photon emission due to the radiative recombination of Wannier excitons is a source of luminescence in semiconductors and QC effects are seen when the size of a particle such as Si-QD approaches the exciton Bohr radius.

1.2 Quantum Confinement

As mentioned in the previous section, the optical properties of nanostructures differ from bulk materials due to spatial confinement of electrons and subsequent broadening of energy levels within the particle. This spatial confinement results in structures such as silicon quantum dots behaving like individual atoms with quantized energy levels rather than a collection of atoms with degenerate energy levels. Bulk material properties like degenerate energy levels give way to quantum properties such as discontinuous energy bands and increased bandgap energy caused by the confinement of electrons in up to three dimensions. Quantum Confinement (QC) effects are apparent as the object dimension or quantum dot diameter in this case approaches ~5nm. Photoluminescence typical of QC is usually in the red region of the visible spectrum (750 – 900nm) for Si-QD in SiO_2 (Yu 1998).

1.3 SiO_2 Defects

The presence of defects around Si-QD and in SiO_2 films can have a significant influence on the electronic and optical properties of Si-QDs. Defects studied here are caused by the irradiation process. An intrinsic point defect may be classified as a vacancy or a self-interstitial defect. A vacancy defect occurs when an atom is knocked out of position, breaking bonds in the process. An interstitial defect occurs when additional atoms (possibly knocked out of place by incoming Si ions) occupy interstitial spaces in the SiO_2. Either oxygen or silicon can be displaced during ion irradiation, breaking Si-O bonds causing silicon and oxygen vacancies and silicon or oxygen excess in different regions. During Si-QD growth, defects occur at the interface between Si-QDs and the surrounding SiO_2. These defects are a byproduct of the crystallization process resulting in dangling bonds with unpaired valence electrons which can quench photoluminescence by acting as non-radiative recombination centers (Lee 2012). The oxide species SiO_3 with one unpaired electron can act as an electron-hole trap at the Si-

QD/SiO_2 interface. It is possible that the size and shape of the quantum dots is affected by the number of vacancies present in the SiO_2 before crystallization. During ion implantation the implanted Si ions cause damage to the SiO_2 film. This damage results in vacancies where a Si or O atom has been knocked out of position and leaves a vacancy behind which isn't filled by another atom. During the annealing/crystallization step after implantation these vacancies are filled by diffusing Si forming quantum dots.

1.3.1 Dangling Bonds

A dangling bond occurs in SiO_2 when a silicon or oxygen atom is out of place and unpaired electrons exist. These sites act to quench PL in unpassivated samples as unpaired electrons trap holes and prevent radiative recombination of electron-hole pairs. Dangling bonds are present at the Si/SiO_2 interface and in areas where the SiO_2 has been damaged due to irradiation with silicon ions. Unpaired electrons are present at each dangling bond site due to atomic vacancies. Hydrogen passivation can deactivate the unpaired electrons to significantly reduce the number of dangling bonds present after crystallization. Hydrogen atoms diffuse into the SiO_2 film and terminate dangling bonds. Determining the number of dangling bonds can indicate the scale of damage caused during implantation which is thought to affect the formation of silicon quantum dots in SiO_2. Damage to the SiO_2 host could free up excess silicon for the formation of Si-QDs and at the same time control nucleation sites which may have an influence on the Ostwald ripening process during Si-QD formation. Defect-mediated diffusion of silicon atoms during the Si-QD growth process may also mean that the presence of defects in the SiO_2 can influence Si-QD growth and cluster formation (Mokry 2009). Damage can be induced before Si-QD growth to investigate the influence of defects.

1.4 Defect luminescence in SiO_2

SiO_2 is transparent in the visible spectrum and has a large energy bandgap of ~9eV. Mid-bandgap energy levels result in luminescence due to electron transitions between localized states and valence/conduction bands and vice versa.

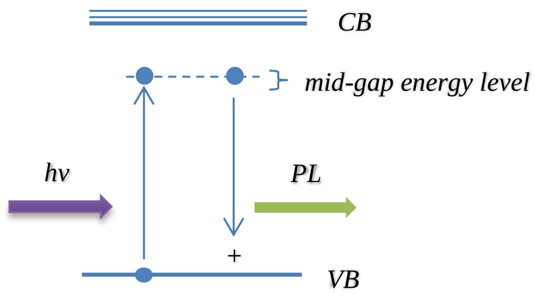

Figure 4: Photoluminescence as a result of mid-bandgap energy levels caused by defects in SiO_2 film.

Interface states can act as electron and hole traps which quench actual Si-QD emission. Defect PL in SiO_2 emits higher energy/shorter wavelength light than Si-QDs with emission in the blue/green region of the visible spectrum as opposed to Si-QD typical red luminescence.

1.5 Thesis Overview

Due to many simultaneous processes during Si-QD photoluminescence in SiO_2 extracting information from characterization techniques can be complex. The aim of this work is to determine whether defects in the host material (SiO_2) have an influence on the growth and/or PL associated with Si-QDs in our samples. Defects and Si-QDs are investigated using Electron Paramagnetic Resonance and PL spectroscopy in order to determine how Si-QD growth and PL emission are affected by defects in SiO_2. QC effects of Si-QD or interface states on the surface of Si-QDs are also investigated. If damage to the SiO_2 film during implantation affects the growth of Si-QDs then it is possible that Si-QD growth can be controlled by pre-implant damage induced in the SiO_2. If defect-related PL is present, it may have an influence on Si-QD PL. A number of different preparation conditions are used to grow Si-QDs in SiO_2. Results of characterization techniques are assessed to form a more complete picture of processes involved in the growth and properties of Si-QDs and the consequence of the abundance of defects present in SiO_2 due to ion irradiation. Defect-mediated diffusion of silicon atoms and subsequently silicon nanoparticles during the Si-QD growth process could have an influence on the distribution and size of Si-QDs in SiO_2. If this is the case then altering the structure of the SiO_2 layer before implanting the Si-QD seed layer should have an influence on the growth of Si-QDs in samples. Differences in Si-QD properties if present should be noticeable by measuring the PL spectra and radiative lifetimes of samples while varying preparation conditions. In this research Photoluminescence spectra, Time Resolved Photoluminescence lifetime and Electron Paramagnetic Resonance characteristics are compared using different pre-implant conditions and the results are discussed.

Chapter 2

2 Implantation and Growth

Silicon quantum dots are grown in an amorphous thermal oxide film of SiO_2 in this research. Silicon ions (Si^+) are implanted into the oxide film at a predefined depth and dose. Annealing promotes the growth of the silicon quantum dots and removes damage to the oxide film which occurs during implantation. A further anneal step is carried out in forming gas (5% H_2: 95% N_2). At 500^oC hydrogen diffuses into the SiO_2 film and terminates bonds which were broken during ion implantation. Broken bonds with unpaired electrons act as luminescence quenching sites. Elimination of these quenching sites results in increased luminescence intensity.

2.1 Thermal Oxide Film Growth

The thermal oxide SiO_2 film used in this work is an amorphous thin film grown using wet thermal oxidation of a crystalline silicon wafer to a depth of 280nm. This material is used since it allows nucleation of Si-QD during annealing and a large difference in band gap energy between SiO_2 (insulator) and Si-QD can result in photoluminescence with lower probability of quenching by SiO_2 host material.

Thermal oxide films used in this research were not grown on site. The following is a brief description of the thermal oxidation process. Wet thermal oxidation of silicon wafer is achieved by exposing a silicon wafer to high temperatures in the presence of pure steam. Crystalline silicon (c-Si) wafers are held vertically or horizontally in a tube furnace during the process. Oxygen and hydrogen gasses are combined and heated to high temperatures ($>800^oC$) at which point they ignite. This reaction results in the production of very high purity steam. The steam is then directed into the furnace chamber with the c-Si wafer(s). Once the steam reaches the wafer surface an oxidation reaction occurs, in which silicon atoms form covalent bonds with oxygen atoms to form

SiO_2. As the film thickness increases the oxidation process slows down. The slowdown in this process is due to the fact that oxygen must diffuse through the oxide film to bond with silicon atoms. Diffusion speed can be increased by increasing the processing temperature but in order to ensure uniform and stoichiometric oxide growth the temperature is kept constant, a 250nm film may take up to 24hrs to grow (Kang 2006).

2.2 Ion Implantation

Ion implantation is used in the Integrated Circuit (IC) manufacturing industry to modify semiconductor materials. Using various elements the electronic properties of semiconductors may be controlled and enhanced. For example, intrinsic semiconductors (e.g. Si, Ge) have an equal number of electrons in their conduction band as holes in their valance band at room temperature. Silicon has a relatively low bandgap (1.1eV) relative to an insulator such as SiO_2 (~9eV) but thermal energy at room temperature is insufficient (k_BT = 25meV@RT) for electrons to make it into conduction band so silicon does not have sufficient charge carriers at room temperature to allow for significant current flow. Using ion implantation intrinsic semiconductors can be altered to have an excess of charge carriers, increasing concentration by up to several orders of magnitude to allow vastly increased conduction. Implanted dopants can be n-type or p-type; acting as electron donor or electron acceptor respectively within the silicon crystal lattice. For example a dopant such as boron (p-type) is implanted beneath the surface of an intrinsic semiconductor wafer such as silicon. Boron atoms act as electron acceptors in the otherwise highly pure c-Si resulting in a p-type semiconductor with an excess of holes or positive charges at room temperature. Si-QDs can be relatively easily grown using ion implantation to implant silicon ions into SiO_2 (Shimizu-Iwayama 1994). In this work silicon ions are implanted in a thin film of SiO_2 to create an excess of silicon in the host SiO_2. These excess silicon atoms allow the formation of Si-QDs in the SiO_2 film.

2.2.1 Implantation Process

The ion implanter consists of a number of sections including sputter source, low energy magnet, accelerator and implantation chamber. A schematic of the 1.7MV Tandetron Accelerator at the University of Western Ontario (UWO) is shown in Figure 5 with the various stages labeled. At the ion source the ions necessary for implant are extracted from the source surface. Ion sputtering is used to extract ions for use in implantation in this research. A cesium source is ionized and Cs^+ ions are accelerated towards a cooled target consisting of the element to be implanted e.g. silicon. The idea behind cooling the target is so that a thin layer of cesium coats the target surface, which aids the sputtering process. The target surface is then sputtered due to bombardment with Cs^+ ions and negative target ions are ejected. The negative ions are injected into the main accelerator chamber where a stripper gas strips electrons to form positive ions (e.g. Si^+). In the main accelerator chamber ions are accelerated to various energies from 50keV to above 1MeV. Implant energies upwards of 1MeV using a medium energy medium current implanter causes beam current drop off so that achieving an appropriate dose can be prohibitively slow.

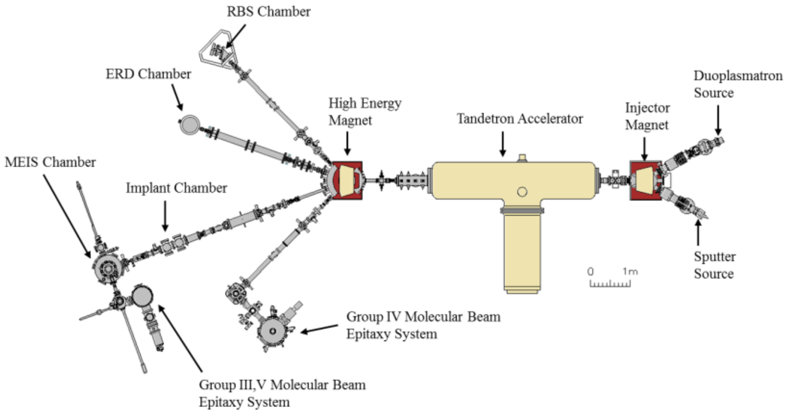

Figure 5: 1.7MV Tandetron Accelerator Schematic (Goncharova 2013)

Only ions of the correct charge, mass and energy are wanted for implant so the beam passes through a high energy magnet which selects ions based on those criteria. By applying the correct magnitude of magnetic field the required ions are directed into the final beam line toward the implant stage. Multiple exit lines are connected to this point to allow for different ion trajectories to be selected. The beam line marked in red in Figure 5 was used in this work. In order to implant more area without moving the sample stage the beam passes through a raster scanner before reaching the sample surface. The sample stage area is under vacuum during. This allows rapid pump down of the sample chamber to reduce time spent loading and unloading the sample. Implantation is through a circular aperture which is changed according to the desired implant area, up to $5cm^2$ is possible. Charge build up at the sample stage can cause positive ions to be deflected resulting in non-uniform implant therefore the sample is supplied with electrons to neutralize charge. Implant Energy as well as ion mass determines the implant depth profile. Increasing beam energy results in a deeper depth profile for a given ion species but more massive ions result in a shallower depth profile for a given beam energy. For example Si^+ into SiO_2 at 50keV implant energy will result in a peak concentration at around 100nm below the SiO_2 surface. 90keV beam energy will peak at around 120nm – 130nm depth. Dose depends on beam current during the implantation process. High beam current means higher beam flux and a higher concentration of the implanted element in the sample resulting in lower ion energy due to the larger number of ions to be accelerated. Medium current/medium beam energy implant will result in a lower dose with a deeper depth profile and high energy implanters use low dose for deep implantation. Damage to the target material during ion implantation occurs due to collisions between incoming ions and the target. Energy transfer from implanted (incident) ions during impact causes subsequent collisions between nearby host (secondary) atoms resulting in a damage cascade effect. For each single incident ion multiple atoms in the host are displaced as each secondary ion transfers kinetic energy to surrounding atoms. Collisions result in vacancy and interstitial defects in the sample. Just as implanted ion concentration has a concentration profile with a peak at a certain depth there is a similar vacancy profile with a peak concentration of vacancies/damage to the target. These profiles can be estimated using Monte Carlo simulations run using Stopping Range of Ions in Matter (SRIM) (Ziegler 2013) software in order to estimate damage expected with ion/target and energy/dose combinations. Peak damage profiles will sit nearer the surface than concentration profiles. Multiple energy implants can be used to investigate the influence of damage in the SiO_2 film on the growth of Si-QD. First a high energy implant is performed which passes through the SiO_2 film into the silicon substrate to induce damage and afterwards a lower energy implant seeds the Si-QD growth in the SiO_2 film. Using this technique the damage can be controlled and quantified to relate subsequent characteristics of Si-QD grown to different pre-implant damage profiles.

2.3 Thermal Annealing

In IC manufacture Rapid Thermal Annealing (RTA) is used to activate dopants (Kuhn 2010) and recrystallize areas of the silicon substrate which were damaged during implantation. In this work thermal annealing is used to repair damaged SiO_2 films and enable growth of Si-QD. RTA is normally performed for only very short durations of seconds at a time. Annealing here is done using a tube furnace and for this reason anneal times are significantly longer and can be up to 2hrs since it is not a rapid thermal anneal (Barbagiovanni 2011). In order to prevent further oxidation of the sample the initial anneal step is performed in a nitrogen atmosphere at a temperature of 1100^{o}C for 2hrs. The second anneal stage is performed at 500^{o}C and in a hydrogen/nitrogen atmosphere of Forming Gas. At this temperature hydrogen diffuses into the SiO_2 film and passivates broken bonds (Dabrowski 2000).

2.3.1 Si-QD Growth

Nucleation of quantum dots occurs in the implanted region in the SiO_2 film during thermal annealing in the tube furnace at 1100^{o}C. Although Si-O bonds occur preferentially, the low diffusion rate of Si in SiO_2 means that Si-Si bonds occur in the silicon rich areas resulting in a buried layer of Si-QD in SiO2. Growth of the quantum dots occurs due to Ostwald Ripening as larger quantum dots grow at the expense of smaller ones. Small quantum dots with a larger surface area to volume ratio are less energetically stable than larger quantum dots. When the excess silicon is used up this process will slow. As long as silicon is available to diffuse towards quantum dots the average size will grow hence lower concentration implants result in smaller Si-QD average size. It is possible that defect-mediated diffusion of Si atoms could have an influence on the formation of silicon quantum dots in SiO_2 with quantum dots forming in areas where damage has occurred and broken bonds are present (Mokry 2009).

2.3.2 Hydrogen Passivation

Passivation of dangling bonds is achieved as the last stage in Si-QD synthesis process. A dangling bond is an unsatisfied valence on an immobilized atom. Hydrogen diffuses into the SiO_2 and eliminates dangling bonds by taking the unpaired electron into a bonding orbital. After the growth stage anneal in N_2 for 2hrs at 1100^{o}C the samples are annealed at 500^{o}C in forming gas (5% H_2/N_2) for 1hr. Forming gas is used in order to eliminate the possibility of spontaneous combustion of hydrogen by mixing it with an inert gas such as nitrogen. At 500^{o}C hydrogen diffuses into SiO_2 and bonds with any available Si atom which has an unpaired electron by forming covalent bonds. A structure which is created during the irradiation process and passivated by hydrogen during this annealing is a silicon atom bonded to three oxygen atoms with an unpaired electron in a sp3 orbital. This is present both in the SiO_2 and at the Si-QD/SiO_2 interface and has been found to be an electron-hole trap site which quenches radiative emission. Fewer unpaired electrons present increases the probability of radiative recombination by eliminating mid-bandgap electron/hole traps where non radiative recombination can occur. As shown in Table 2 in Chapter 4 samples were prepared with two stages of annealing. Stage 1 is a sample set 1-5 with no hydrogen passivation and Stage 2 is a sample set 1-5 with hydrogen passivation. These samples were prepared in order to compare EPR spectra and PL spectra for both hydrogen passivated and non-passivated samples.

Chapter 3

3 Experiment

Thermally grown oxide films of 280nm thickness were used as a host material for Si-QD. These films were sourced from Silicon Sense Inc. The SiO_2 films were implanted at room temperature with Si^+ ions at energies of 90keV, 400keV and 1MeV. The projected peak implant depth of Si^+ within the SiO_2 film and c-Si substrate beneath was estimated using SRIM simulation software to be 148nm, 654nm and 1.38µm respectively. Only the 90keV implant range is within the 280nm SiO_2 film. Prior to implantation the silicon wafers were cut using a diamond tip scribe into ~5cm^2 pieces for mounting onto the implant chamber stage. A 5cm^2 implant area was used for the 400keV and 1MeV samples and a 3cm^2 implant area was used for the 90keV sample with lower dose. Different implant areas were used due to the implant dose chosen, a higher implant dose requires more implant time therefore the smaller implant area was used for the 90keV sample with lower dose. Ion dose for the 90keV implant was $1x10^{17} ions/cm^2$ with $1x10^{16} ions/cm^2$ used for both the 400keV and 1MeV implants. All implants carried out are listed in Table 1. Each energy/dose was implanted onto an individual wafer so that reference samples could be kept. After implantation, samples were cut into 1cm^2 sections in order to allow for different preparation stages to be compared. Si-QD growth was carried out in a quartz tube furnace at 1100^{o}C for duration of 2hrs in a high purity nitrogen atmosphere. The tube furnace was pumped down to ~50mTorr with a roughing pump and nitrogen gas was allowed to flow through according to the procedures supplied. The furnace heater was programmed according to the operation manual supplied, allowing 50min for ramp up to 1100^{o}C, 2hrs at the required temperature and approximately 3hrs for cool down. During ramp up and cool down periods the samples were placed inside the quartz tube but outside the heated area in order to ensure that the anneal time was 2hrs and no longer. During the temperature ramp up it is important to monitor gas flow as it fluctuates as the temperature increases, usually two adjustments are necessary to ensure that gas flow remains constant during ramp up. A nitrogen atmosphere was maintained in the furnace during cool down. Next a hydrogen passivation anneal was carried out to reduce the effects of non-radiative electron-hole recombination. Each sample was annealed in forming gas (5%H_2:N_2) at 500°C for 1hr. Between the growth stage anneal and the hydrogen passivation step, samples were left inside the furnace and the same procedure for preparing the furnace atmosphere was followed, this time with forming gas. The same temperature ramp up procedure was followed, this time maximum anneal temperature was set to 500°C.

PL spectroscopy sample size was 1cm^2. These measurements were performed at McMaster University, Hamilton. The excitation source is a 2mW continuous power 325nm HeCd laser with 1mm beam diameter and intensity of ~64mW/cm^2. The beam is passed through a ½" aperture onto the sample without focusing. The PL emission is collected by an achromatic objective lens and focused into a fiber optic patch by an achromatic lens. The optical fiber is Ocean Optics model QP600-2-VIS-NIR. The spectrometer is an Ocean Optics model ADC1000 and is connected to a PC. Ocean Optics software is used to collect and process the data. Origin Pro 8 software was used to correct and smooth the data afterwards. No special sample preparation was undertaken for these measurements and they were carried out at room temperature.

TRPL spectroscopy was performed at room temperature using a pulsed 405nm laser diode as the excitation source. The laser driver is a 405nm laser diode driver with potentiometer and Transistor-Transistor Logic (TTL) switching purchased from O-Like lasers (www.o-like.com). The TRPL set up is housed in a light sealed box, measurements were taken with lab lights on and off and no difference was observed. The experimental set up was identical to that shown in Figure 7 with a 450nm high-pass Thorlabs filter placed in front of the PMT in order to filter out reflected UV light from the sample. The laser was focused onto the sample using a focusing lens to create a beam diameter of ~1mm at which point the most intense PL was observed in the each sample. The waveform generator was set to a pulse frequency of 500Hz with 200μs pulse width. Although higher frequency pulsing would allow a larger sample rate, 500Hz was selected in order to extend laser diode life. PL emission was collected using a Hamanatsu R7400U-20 Photomultiplier Tube (PMT) set to -800V and output measured with a Cleverscope CS328A digital oscilloscope. A Trigger signal was taken to Channel B of the oscilloscope from the waveform generator using a T-connection. Each sample was irradiated for 2min before the decay trace was saved. Exponential averaging with 20 frame sample storage was used with 14bit sampling.

Samples selected for ESR measurements were removed after the growth anneal step and before the passivation step. All PL spectroscopy was performed before ESR measurements were taken since ESR requires a smaller sample size therefore further cutting of the samples. ESR spectroscopy measurements were performed with a Jeol JES-FA200 system at room temperature on unpassivated samples. Sample preparation for ESR spectroscopy involved further sectioning of samples into 4mm x 7mm pieces due to the sample size needed to fit into the quartz tube for ESR measurements. After cutting the samples were sonicated in a sonic bath for 15min in order to remove any contamination. Each sample was placed in the ESR system under vacuum. ESR measurements were then collected with the sample exposed to a DC magnetic field varying between 328mT and 340mT which causes the splitting of singly-occupied electron energy levels into sublevels corresponding to parallel and antiparallel electron spin orientations and an AC field at a frequency of 9.5GHz which induces optical transitions between these sub-levels. The resultant spectra were collected and graphed using Origin Pro 8 graphing software. No further modeling has been done on these spectra as of yet.

4 Characterization Techniques

Photoluminescence Spectroscopy and Time-Resolved Photoluminescence Spectroscopy (TRPL) are non-destructive characterization techniques used here to probe electronic states in Si-QD/SiO_2 films. Both Si-QD and defects in SiO_2 show photoluminescence (PL). For the most part they emit light in different spectral regions and so are distinguishable with PL Spectroscopy although some Si-QD/SiO_2 interface states exhibit PL at a similar wavelength (red) to Si-QDs (Pacchioni 2000). TRPL is a more specific tool bringing with it more complex data. Interpreting radiative decay lifetimes involves multi-exponential fitting of Photo Multiplier Tube (PMT) decay traces in order to extract information regarding mechanisms. Si-QD/SiO_2 films contain defects, oxide interfaces and quantum dot clusters each possibly contributing to the PL radiated. Electron Paramagnetic Resonance (EPR) is a technique used here to investigate the electron spin of atoms in Si-QD/SiO_2 films. Paramagnetic defects contain unpaired electrons which can be detected using EPR. Depending on the strength and shape of the EPR signal collected, different the types of dangling bonds can be identified as each unpaired electron is affected by its local environment i.e. the surrounding atomic species.

4.1 Photoluminescence Spectra

Photoluminescence spectroscopy involves irradiation of a sample with light in order to cause interband electronic transitions. Light emitted by the sample is then collected and displayed as a spectrum using a spectrometer. It is a non-destructive method for investigating the electronic structure of materials by irradiation with UV-Vis-IR radiation. PL spectroscopy is a relevant experimental method in this research as it can be used to identify defects in oxides and to characterize semiconductor nanostructures. Photoemission from these materials can provide information about concentrations of defects and size distribution of nanostructures under various preparation conditions. Due to QC effects, nanostructures like Si-QDs can emit energy in the form of photons which gives information about their properties and the surrounding host material. PL spectroscopy is a common tool for investigating Si-QD and silicon nanoclusters and studies have been carried out on luminescence of nitride passivated silicon nanoclusters (Wilson 2011), non-radiative recombination centers in silicon in silicon nitride (Gritsenko 1999) and rare earth metals (Kudo 1997) to name but a few. PL spectroscopy normally is performed at room temperature. Alternatively if sample cooling is necessary only the sample stage needs to be cooled.

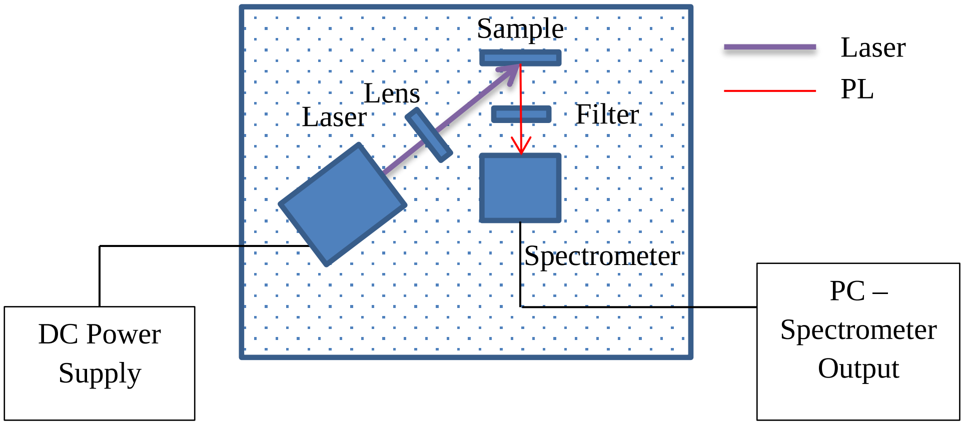

Figure 6: A PL Spectroscopy Set-up

A typical PL Spectroscopy set up includes an excitation source such as a laser. The excitation laser wavelength is sample dependent in that the photon energy must be higher than the bandgap energy of the material under investigation. A mirror is used to direct the laser beam onto the sample so that the beam spot can be easily adjusted without disturbing the laser housing. A lens or lenses are necessary to focus the emitted light from the sample into a spectrometer for light collection. Fixed or variable wavelength lasers are used to excite electrons in the sample material from the valence band into the conduction band and the intensity of emitted light is recorded as a function of wavelength. Photoemission due to interband electronic recombination is the source of light collected at the spectrometer. Direct bandgap semiconductors exhibit photoluminescence upon the absorption of a photon. As mentioned in Section 1, photoluminescence is not a usual characteristic of indirect bandgap semiconductors such as bulk crystalline silicon, but nanostructures such as Si-QDs in SiO_2 do exhibit strong PL at room temperature when excited with UV light (Mokry 2009). PL spectra due to defects and oxide interface states at the Si-QD/SiO_2 interface are dominated by low intensity emission wavelengths in the visible spectrum but blue shifted (500*nm* – 600*nm*) in comparison to PL due to QC effects (700*nm* – 900*nm*) in Si-QD structures. Radiative recombination of electron-hole pairs in due to defects has a shorter emission wavelength since the energy bandgap is larger resulting in higher energy emission. Defect related PL can indicate the concentration of defects in a sample due to damage during ion irradiation. While defect PL is eliminated by annealing and hydrogen passivation it is thought that knowledge of the concentration of defects in a sample prior to the Si-QD growth stage can help to understand more about the growth mechanisms of Si-QDs in SiO_2. PL spectra and Time Resolved PL are the two main experimental techniques used here to characterize Si-QDs in SiO_2.

4.2 Time-Resolved Photoluminescence

Time-resolved Photoluminescence (TRPL) spectroscopy is based on the same physical principles as PL spectroscopy in that excitation of the sample with light causes interband electronic transitions resulting in photon emission due to electron-hole recombination. Time-resolved PL spectroscopy is used extensively to identify QC effects or to distinguish QC based emission from defect related PL in SiO_2 (M.Dovrat 2004) (Dohnalova 2009). In PL spectroscopy a continuous wave (CW) laser is used as an excitation source and the wavelength of photons emitted is recorded. In TRPL spectroscopy measured here the radiative lifetime of emission is observed using a pulsed laser source, PMT and digital oscilloscope. Radiative recombination lifetimes of Si-QDs in SiO_2 are an area attracting attention in the last decade although debate as to exactly what mechanisms are involved and how the resultant data should be interpreted is ongoing. As an experimental technique this method can provide information on Si-QD properties as a function of growth conditions. The radiative lifetime (τ) varies depending on Si-QD size. QC lifetimes have been found to have a size dependent range between $20\mu s$ – $140\mu s$ (Garcia 2003) but whether this is due only to QC or includes interface and defect related PL is debatable. High resolution measurements necessitate shorter pulse widths on the order of nanoseconds for excitation in order to record equally short decay lifetimes but longer lifetimes from $20\mu s$ upwards can be observed with a longer pulse duration (μs) setup.

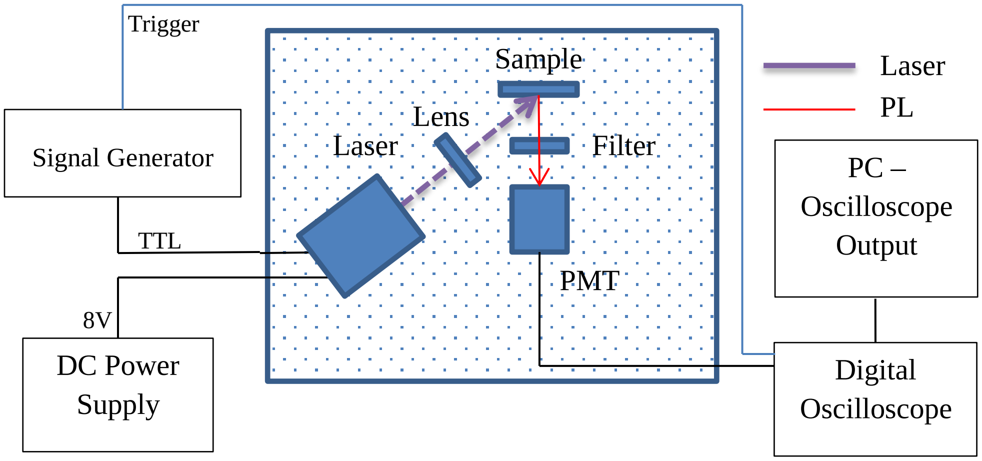

Figure 7: Time Resolved Photoluminescence Set-up

QC related PL emission from Si-QD is a quasi-direct process due to the fact that there is a high probability of radiative recombination. It is described here in terms of direct gap transitions. The radiative lifetime (τ) of observed decays vary depending on contributing structures, interface states, vacancy defects or QC from Si-QDs. During laser excitation an electron absorbs energy from an incident photon supplied by the excitation source, and is promoted from the ground state at the valence band (VB) to an excited state above the conduction band (CB). Due to the promotion of the electron a hole is created at the VB energy level. The electron goes through a number of rapid (ps) relaxation processes. Excess (>Eg) energy dissipates to the lattice and the electron relaxes to the edge of the bandgap corresponding to this lowest energy level in the CB. During the radiative recombination process the electron decays back to the ground state (VB) and in doing so emits energy in the form of a photon with energy corresponding to E_g. TRPL measures the length of time over which radiative processes like this occur. Relaxation times above the conduction band where energy is lost as heat are fast enough to be negligible; the most important information is contained in the length of time emission occurs after the excitation source is turned off.

4.3 Electron Paramagnetic Resonance

Electron Paramagnetic Resonance (EPR) is used to study paramagnetic centers indicative of unpaired electrons in ions and molecules. Its principles are similar to those of Nuclear Magnetic Resonance (NMR). While the NMR spectrum is a result of nuclear spin, as the name suggests the, EPR spectrum is the result of the electron spin magnetic moment. NMR has a wide variety of uses especially in the medical. Any element with nuclear spin can be investigated using NMR whereas in the case of EPR not all materials will have unpaired electrons. In materials that do contain paramagnetic centers such as unpaired electrons in dangling bonds, EPR is a powerful tool since it can probe highly specific regions such as nanostructures. Paramagnetic defects are significant in that they are caused by paramagetism due to unpaired electrons.

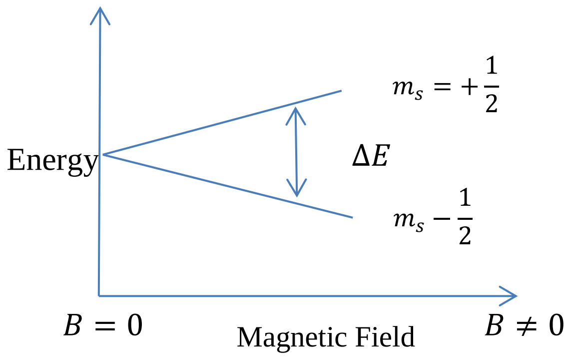

Figure 8: Zeeman Splitting in EPR showing energy level splitting $(\Delta \boldsymbol{E})$ with increasing magnetic field energy (B).

Electron spin magnetic moment is highly dependent on its surroundings and interactions with other species in a given sample so the resultant EPR spectrum is sensitive to sample preparation and external interference which can cause noise in the signal. Observable features which are of interest in this study include interfacial oxide states (Si-QD/SiO_2) and defects containing dangling bonds with unpaired electrons where atoms (Si or O) have been displaced due to ion irradiation. An electron has a spin magnetic moment (m_s) due to spin about its axis represented by $m_s = \pm\frac{1}{2}$ depending on orientation. Electrons in full or bonding orbitals are paired, one spin up and one spin down, according to the Pauli Exclusion Principle. This paired configuration is diamagnetic, meaning one electron is in the $m_s = -\frac{1}{2}$ state and the other electron is in the $m_s = +\frac{1}{2}$ state. An unpaired electron will be paramagnetic meaning that a single unpaired electron will be either in the $m_s = -\frac{1}{2}$ state or in the $m_s = +\frac{1}{2}$ state with no opposite spin electron present. Unpaired electrons can be detected using EPR spectroscopy. In the presence of a magnetic field previously degenerate energy levels split due to the Zeeman Effect. Electron transitions can now be induced from lower to higher energy levels through the absorption of energy. Usually the magnetic field is varied in the presence of a fixed microwave frequency in the region of *9GHz*. As the magnetic field increases, the difference in the energy levels widen, and when the difference (ΔE) between the two levels equals the energy supplied by the microwave signal (hv), absorption occurs. Usually the first derivative of the resultant absorption spectrum is displayed. Without the presence of the microwave signal the unpaired electrons are distributed almost equally between $m_s = -\frac{1}{2}$ and $m_s = +\frac{1}{2}$ according to the Maxwell-Boltzmann law. When the resonance condition $hv = \Delta E$ is met, unpaired electrons transition from the lower energy level to a higher energy level and in the process must change spin from the $m_s = -\frac{1}{2}$ state to the $m_s = +\frac{1}{2}$ state. The EPR spectrum resonance condition will depend mainly on spin-orbit coupling. An unpaired electron is promoted to $m_s = +\frac{1}{2}$ and relaxes back to $m_s = -\frac{1}{2}$ in a short period of time so that electrons in $m = -\frac{1}{2}$ state, and electrons in the $m_s = +\frac{1}{2}$ state do not equalize. Spin-lattice relaxation occurs when energy is lost to the lattice. This is a slower process and is usually negligible. The splitting of energy levels due to the Zeeman effect is directly proportional to the magnetic field strength as shown in Equation 2.

$$\Delta E = hv = g_e\, \mu_B B \tag{4}$$

where ΔE is the difference between energy levels due to Zeeman Splitting. g_e is the proportionality constant between the observed electron magnetic moment and μ_B the magnetic moment of a free electron or Bohr Magneton. A large part of EPR analysis involves the influence of surrounding nuclei on unpaired electron spin. This can give insight into the local environment of the electron i.e. what species it is associated with. PL intensity has been found to be strongly linked to the density of unpaired electrons in SiO_2 (Hiller 2010). A difference between the existence of interface unpaired electrons versus defect related unpaired electrons can indicate the amount of damage to SiO_2.

Chapter 4

5 Results and Discussion

Si-QD samples were prepared using ion beam implantation to seed Si^+ ions in a thermally grown SiO_2 oxide film on silicon substrate. Samples were implanted with three implantation energies and two concentrations of Si^+ ions. Table 1 shows the sample set indicating which samples received double implants and the energy and dose used. Sample 1 was implanted with a single dose of $1x10^{17} ion/cm^2$ Si^+ and implant energy of 90keV. Sample 3 was initially implanted with a dose of $1x10^{16} ion/cm^2$, implant energy of 400keV and subsequently implanted with a single dose of $1x10^{17} ion/cm^2$ Si^+ at an energy of 90keV. Similarly Sample 4 was initially implanted with a dose of $1x10^{16} ion/cm^2$ at an energy of 1MeV and subsequently implanted with a single dose of $1x10^{17} ion/cm^2$ Si^+ at an energy of 90keV. Samples 2 and 5 were implanted with a dose of $1x10^{16} ion/cm^2$ at energies of 400keV and 1MeV respectively. The intention of an initial high energy implant is to induce defects in the 280nm thick SiO_2 film. 400keV and 1MeV implant energies into the silicon substrate cause vacancies and broken bonds in the SiO_2 which could mediate Si-QD growth and influence PL characteristics. PL spectroscopy measurements were performed at McMaster University, Hamilton, Ontario using a 325nm HeCd laser excitation source. TRPL measurements were taken using a 405nm laser diode excitation source at UWO. As illustrated in Figure 6 this set up uses a 405nm air cooled laser diode as excitation source and a Hamamatsu R7400U-20 PMT for light collection. A 450nm high pass filter was placed between the sample and the PMT in order to filter out reflected source light which would oversaturate the PMT and obscure any PL from the sample. The PMT was connected to a Cleverscope CS320A digital oscilloscope which displays two channels A and B. Channel A is the PMT signal and the Channel B signal is taken from the function generator which switches the laser on and off at 200Hz with a variable pulse width. During the initial setting up of the system a 1Ω resistor was added to the laser driver circuit in series and the voltage drop across it was monitored and displayed on Channel B in order to measure the current through the laser diode. Once ideal operating conditions were established Channel B was connected to monitor the TTL pulse signal to the laser. This triggering source is more stable than the previous set up as the voltage drop taken across the resistor was causing interfering with the PMT output signal resulting in deterioration of the signal and excessive noise at on/off points. Extensive measurements were taken to establish the minimum pulse width possible and the overall resolution of the system. Combining the function generator and the TTL-activated laser diode driver, the excitation pulse width could be reduced to as low as 50ns and a clear signal was still detected by the PMT. Increased pulse frequencies serve to speed up data collection but decrease the life of the laser diode. Pulse frequency was not increased beyond 1 kHz for this reason. Sample saturation was found to occur at pulse widths between 120µs and 200µs. Increasing pulse widths from 50ns up to sample saturation were used to test whether pulse width had any influence on the radiative lifetimes. Attempts were made to establish if pulse width and power variations had similar effects.   A trim pot was introduced into the circuit to allow for variable laser power measurements to be taken. The resistor was varied between 0 Ω and 100 Ω in order to observe if there was any variation in radiative lifetime from samples.

5.1 Silicon Quantum dot Photoluminescence

Photoluminescence emission spectra were collected from unpassivated and passivated samples. Stage 1 samples were implanted and annealed but no hydrogen passivation was carried out. At Stage 2 Si-QD are present in the SiO_2 film. Absorption spectra have not yet been calculated for these samples.

Stage 1	No Hydrogen passivation (1)
Stage 2	Hydrogen passivated (2)

Table 1: Passivation Stage 1 and 2.

Figure 9 shows the PL intensity trend between unpassivated and also passivated samples 1,3 and 4. Unpassivated sample PL intensity decreases in with higher energy implant while the passivated samples seem to show a trend towards higher intensity PL with increasing implant energy although the errors associated suggest the need for a larger sample set.

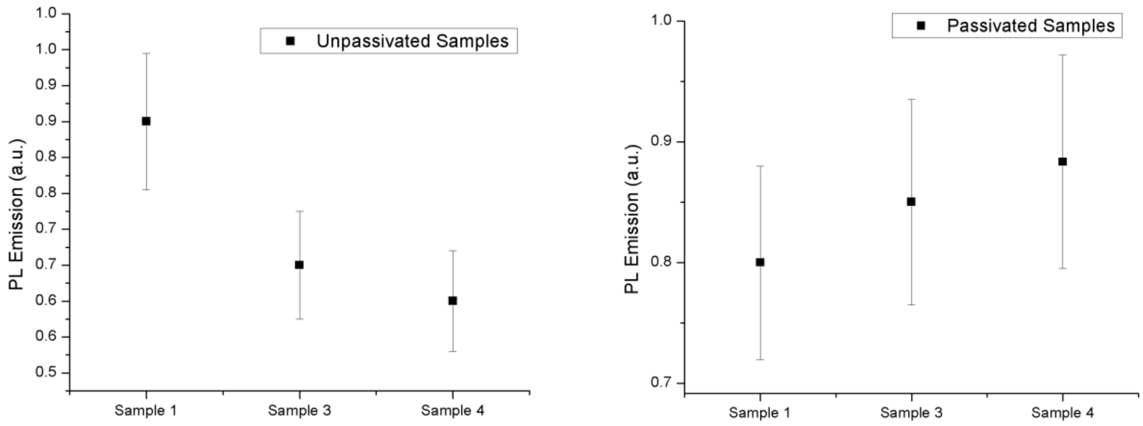

Figure 9: Stage 1 passivation intensity comparison. Double implant Sample 3 and 4 have lower intensity PL than the single implant Sample 1 indicating more quenching in these samples.

Figure 10 shows a comparison of single and double implant samples. Here PL is more intense from the unpassivated single implant 90keV sample when compared to double implant unpassivated samples. Reduced PL in unpassivated double implant samples is most likely caused by mid-bandgap electron-hole traps quenching emission.

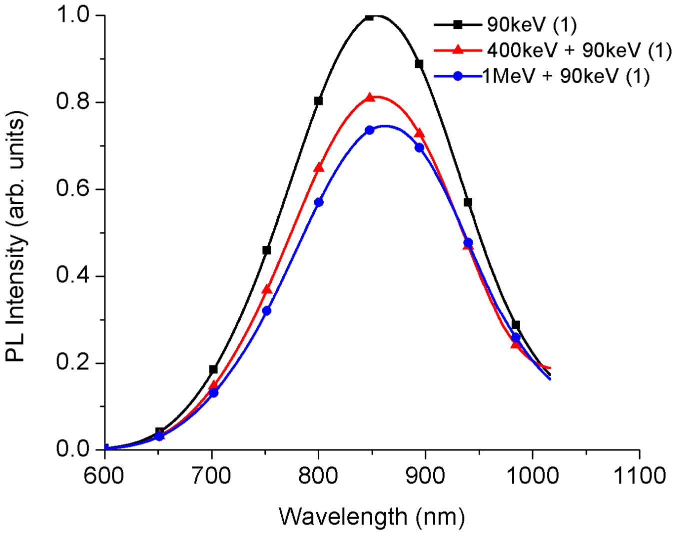

Figure 10: PL of Stage 1 samples, single and double implant with no hydrogen passivation. Highest intensity PL is from 90keV implant Sample 1 and lowest from the 1MeV + 90keV double implant Sample 4. The Y-axis represents the relative intensity of PL based on the most intense sample.

SRIM simulation software was used to simulate the implantation profiles for all implants in order to estimate implant depth profiles and vacancy profiles.

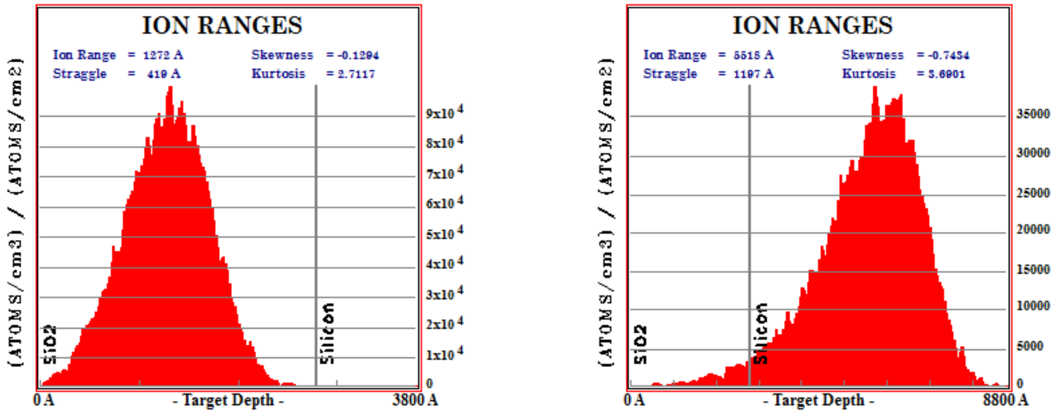

Figure 11: Simulated ion distribution for Sample 2 (right) and Sample 1 (left)

As seen in Figure 11 the peak ion concentration for (90keV) Sample 1 is calculated at 127.2nm (1272 Å) and for Sample 2 (400keV) the implant profile is much deeper given the higher energy at 551.8nm (5518 Å). Importantly for this experiment the concentration of Si^+ in the SiO_2 layer in Sample 2 is low enough to be negligible as is also the case with Sample 4 and 5 implants at energy of 1MeV. Further experimental work needs to be carried out in order to confirm these simulated ion ranges and vacancy plots.

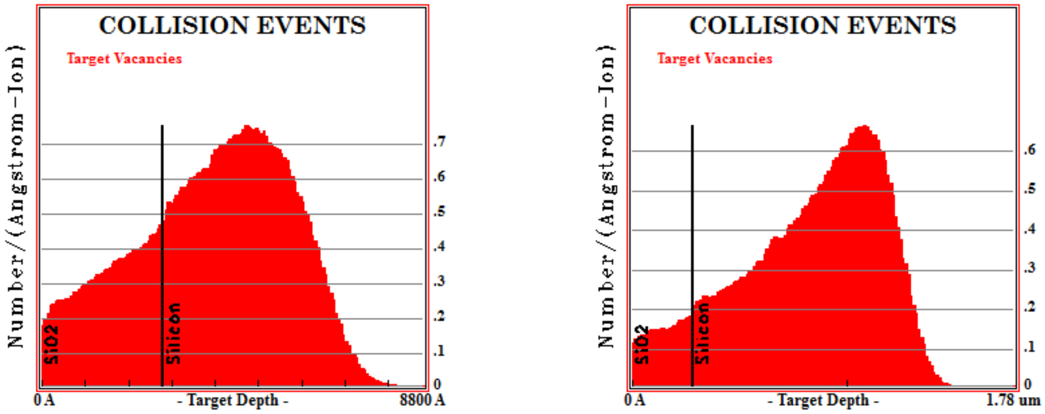

Figure 12: Vacancy profile for Sample 2 (left) and Sample 5 (right)

SRIM vacancy profiles in the SiO_2 film are shown in Figure 12 and are progressively deeper with increasing implant energy. The vacancy profile within the SiO_2 layer is higher, roughly doubled for the 400keV pre-implanted sample when compared to the 1MeV pre-implanted sample due to the deeper damage profile of the 1MeV implant. The ionization profile is larger in the SiO_2 film for the 1MeV pre implant than the 400keV implant. It is possible that the difference in PL intensity between samples is partly due to the ionization profile influence on Si-QD growth. At low energy ion implantation (<100keV) nuclear stopping dominates where target damage is caused by the incoming ions colliding with the nuclei of the substrate material. However for the same ion at higher implant energies electronic stopping dominates where ionization causes heating in the substrate material. This heating is due to ionization of the substrate atoms through collisions with incoming ions. Double implant samples in this work have electronic stopping profiles which are significantly larger in the 1MeV and 400keV implanted samples when compared to the 90keV single implant sample. The unpassivated the single implant 90keV sample shows more intense PL when compared to the double implant samples in Figure 10 indicating more efficient emission from the single implant sample due to less quenching. PL collected from hydrogen passivated samples in Figure 13 and 14 shows the most intense PL in the 1MeV double implant sample followed by 400keV double implant and 90keV single implant respectively. These results show a reversal in intensity order from Stage 1 between the 1MeV and the single implant 90keV sample indicating an improvement in PL efficiency in the sample with a double implant.

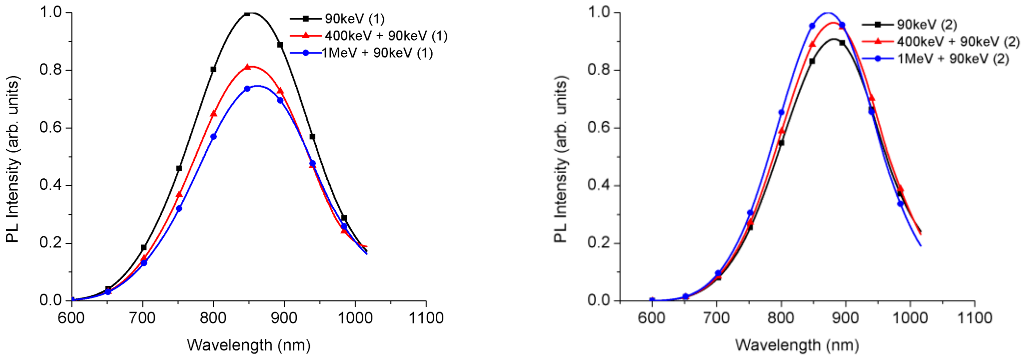

Figure 13: PL of Stage 1 samples (left) with no hydrogen passivation and Stage 2 samples (right) with hydrogen passivation. 90keV single implant is compared to two double implant samples. The Y-axis represents the relative intensity of PL based on the most intense sample from each graph.

Given how close these intensity peaks are to one another and taking into account a 5% standard deviation associated with the raw data more samples need to be tested but the trend does indicate increasing intensity for Si-QD samples grown in SiO_2 in which damage was induced by a high energy initial implant of ions into the silicon substrate which supports vacancy mediated Si-QD growth.

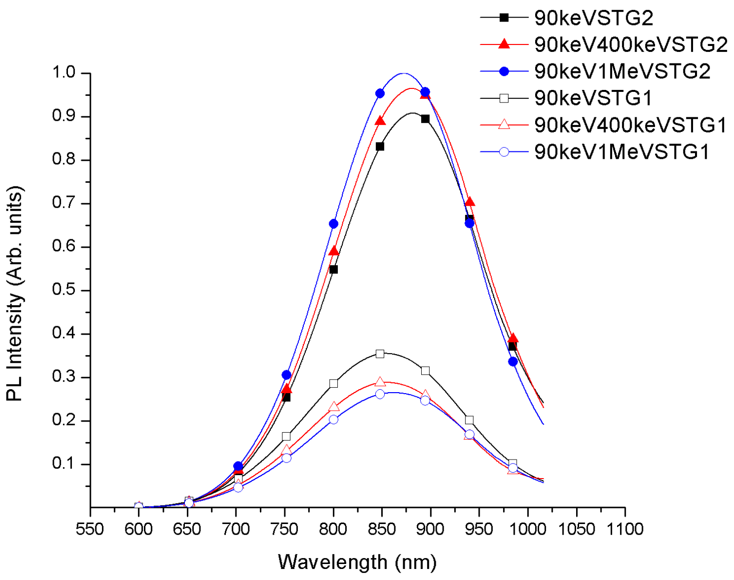

Figure 14: PL emission intensity and emission wavelength comparison between Stage 1 and Stage 2 prepared samples with both single and double implants. The Y-axis represents the relative intensity of PL based on the most intense sample, in this case 1.0 on the graph is equal to the peak intensity of Sample 5.

The sample represented by the blue line (circle markers) in Figure 14 underwent double implantation of 1MeV and then 90keV Si^+ at doses of $1x10^{16}ion/cm^2$ and $1x10^{17}ion/cm^2$ respectively gains most from the hydrogen passivation meaning that some gain in PL intensity is possible due to excess defects already present or induced in the SiO_2 film prior to implantation of excess Si^+ for growth of Si-QD

5.2 Time Resolved Photoluminescence: Decay Lifetimes

TRPL results conducted on Stage 2 samples indicate a slight difference in radiative lifetimes in Samples 3 and 4 but a longer radiative lifetime for Sample 1 when fitted using a stretched exponential fitting model. Pulse duration is 200µs for all TRPL data. These lifetimes indicate larger Si-QD for Sample 1 (single implant) and smaller Si-

QD diameters for double implant Sample 3 and 4. The decay data obtained from experiments using the TRPL set up shown in Figure 15 and 16 are fitted stretched exponential and triple exponential models. Both fitting methods result in a good fit with adjusted r^2 factors of close to 1. The stretched exponential fitting model shown in Equation 3 is used for comparison between samples.

$$I = I_1 e^{-(\frac{t}{\tau_1})^\beta} \qquad (5)$$

where τ is the average relaxation lifetime of the sample and β is the stretching factor limited between 1 and 0. This function assumes an infinite number of decay mechanisms and the resultant average lifetime is used here to compare samples.

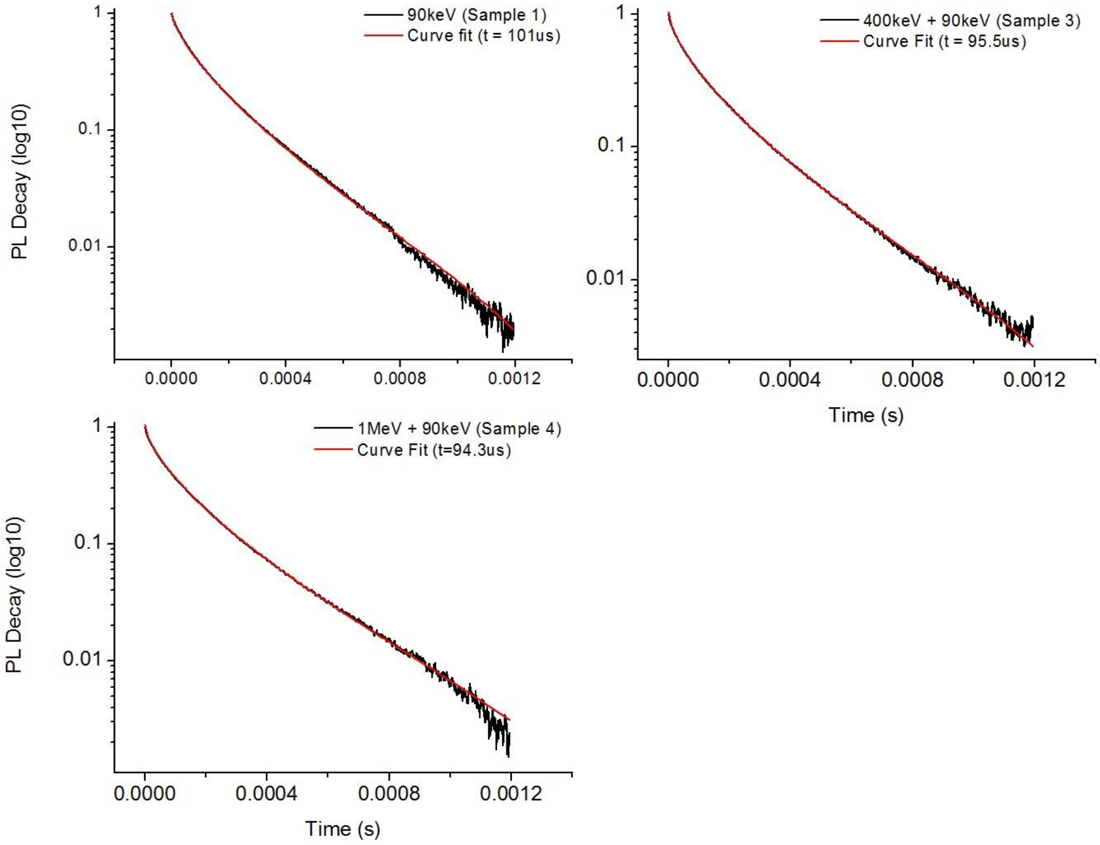

Figure 15: TRPL radiative decay for double implant samples 1, 3 and 4 where $\boldsymbol{\tau}$ is the radiative lifetime modeled using a stretched exponential fit.

Triple exponential fitting is also used and results show a similar trend towards shorter radiative lifetimes with higher energy double implanted samples for the longest radiative lifetime. Plots are shown in Figure 16 and lifetime data in Table 3.

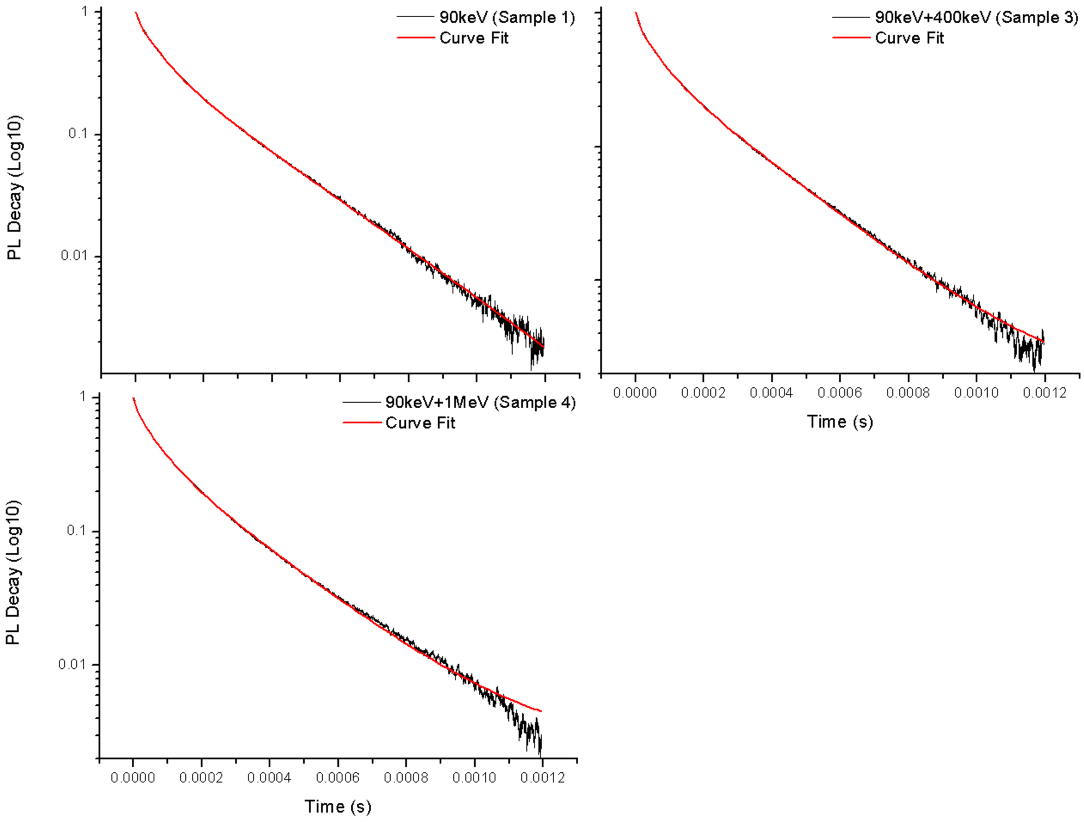

Figure 16: TRPL radiative decay for double implant samples 1, 3 and 4 modeled using a triple exponential fit.

Radiative Lifetimes	**Sample 1 (90keV)** $(^{+}/_{-}\ 5\mu s)$	**Sample 3 (400keV + 90keV)** $(^{+}/_{-}\ 5\mu s)$	**Sample 4 (1MeV + 90keV)** $(^{+}/_{-}\ 5\mu s)$
τ_1	**220**	**212**	**205**
τ_2	**63.6**	**56.1**	**56.1**
τ_3	**9.15**	**7.99**	**8.17**

Table 2: PL radiative lifetime ($\boldsymbol{\tau}_1$) results using triple exponential fit

As seen from the PL Spectroscopy results there is a peak emission wavelength shift between samples 1 and 4 possibly demonstrating different average Si-QD size with larger Si-QD demonstrating longer radiative lifetime emission (Garcia 2003). It is understood that with decreasing Si-QD size comes a blue shift which is evident in these data. Without TEM images as yet it is not possible to definitively say if in fact the average Si-QD size differs between samples but results from PL spectra do show changes in PL emission intensity and a wavelength shift.

5.3 Electron Paramagnetic Resonance: Paramagnetism and Dangling Bonds

Results from EPR are preliminary and given the complexity of the sample and the qualitative nature of the measurements more data and analysis is necessary to develop a clearer picture of paramagnetism as a result of dangling bonds in these samples. What can be seen from the data collected is that when compared to the manganese reference signal the EPR signal from each unannealed sample differs in a way which is to be expected judging by the implant conditions. This information is useful in that it tells us that although a large portion of each sample is made up of the silicon substrate, EPR may still be able to shed some light on the as implanted structure of the samples in the 280nm SiO_2 film region. Figure 17 shows EPR spectra from Sample 1 – 5.

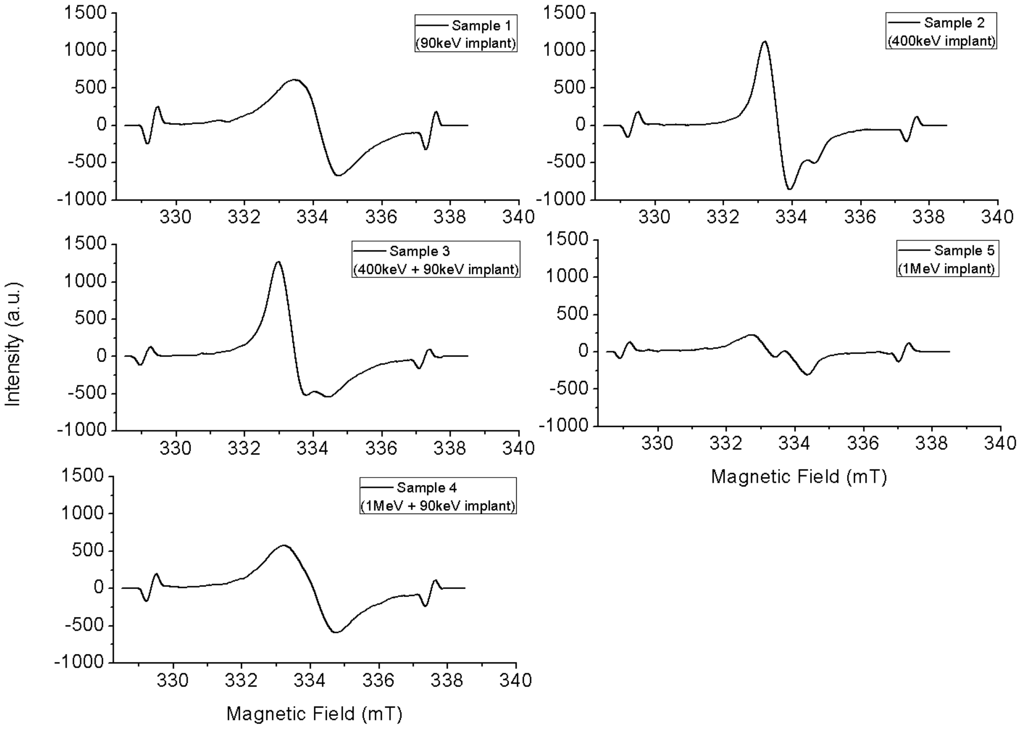

Figure 17: EPR signals from single and double as implanted unannealed samples. g-factors for these spectra have not yet been calculated.

Samples 2, 3 and 5 show a noticeable signal overlap indicating two signals represented by additional peaks in the spectrum, possibly one coming from the 280nm film and the other from the silicon substrate. What is known from SRIM simulations is that there should be a higher vacancy concentration in Sample 3 which underwent a double implant with 400keV implant energy and dose of $1x10^{16} ion/cm^2$and subsequently with 90keV and $1x10^{17} ion/cm^2$ silicon ion dose. Given the SiO_2 structure more paramagnetic dangling bonds with unpaired electrons should be created in the SiO_2 film compared to the silicon substrate. The most pronounced paramagnetic signal indicating a high spin density of unpaired electrons is apparent in Samples 2 and 3. If it is possible to use Samples 2 and 5 in order to subtract their signals from the double implant samples it could be possible to determine the spin densities of the double implant samples in the 280nm SiO_2 film and directly compare different double implant energies of 1MeV and 400keV. With a larger signal from Sample 3 with 400keV and 90keV implants it is possible to assume that this increased signal is the result of a higher number of unpaired electrons in the sample due to damage during the 400keV implant. When this result is considered with the PL spectroscopy results it could indicate that the apparent higher intensity from Sample 3 compared to the single implant 90keV Si-QD Sample 1 is due to defect mediated growth of Si-QD influencing luminescence characteristics. Things become slightly more complicated when looking at Sample 4 which would be expected to have a lower number of dangling bonds in the SiO_2 film than Sample 3 but instead the result is a less intense but broader signal. As before comparing this with PL the spectrum from double implant Sample 4 after anneal suggests defect mediated growth of Si-QD in the SiO_2 film.

Chapter 5

6 Conclusions and Future Work

When all results from this research are evaluated it is apparent that defect mediated growth of Si-QD in SiO_2 does have an influence on PL emission intensity. EPR results, although preliminary, show that damage to the SiO_2 film by high energy pre-implants (400keV and 1MeV) does induce an appreciable increase in the number of unpaired electrons and therefore vacancy defects. Further EPR analysis of unpassivated samples will be carried out at low temperatures to increase signal, and rotational measurements can be taken to differentiate between isotropic and anisotropic dangling bonds. Isotropy indicates vacancy defects in the SiO_2 film while anisotropic signals can indicate the existence of unpaired electrons at the Si-QD/SiO_2 interface. Since it is widely believed that PL intensity in Si-QD in SiO_2 is related to the existence of the oxide interface region of Si-QD it would be useful to attempt to quantify their influence on the wavelength and intensity of Si-QD emission. PL spectroscopy results before and after hydrogen passivation show a trend toward higher intensity PL emission with increasing pre-implant energy for hydrogen passivated samples which is a reversal of the unpassivated PL intensity trend as seen in Figure 9. If defect-mediated Si-QD growth is fully or partially responsible for this increase in emission intensity or whether the ionization profile is also involved needs to be further investigated. It is accurate to say results show that there are differences in PL emission between samples with equal concentrations of excess Si ions implanted in the SiO_2 layer. This indicates that different concentrations of vacancies in the SiO_2 layer affect PL intensity in both unpassivated and passivated samples. Further work could include investigating the Si-QD layer in each of these samples to compare their cross sections by step etching followed by X-ray Photoelectron Spectroscopy (XPS) or by Focused Ion Beam (FIB) sectioning of samples to directly compare how the depth profile and Si-QD size distribution are affected by Si-QD defect-mediated growth. TRPL measurement results show differences in radiative lifetimes between Samples using stretched exponential fitting and triple exponential fitting models; both with good fits. As implant energy and therefore damage to the SiO_2

layer increases; radiative lifetimes decrease. The shortest radiative lifetime was measured in Sample 4 (90keV + 1MeV) as was the most intense PL. Increased PL intensity suggests a higher concentration of Si-QD in the SiO_2 film with induced defects. Shorter radiative lifetimes suggest a shift towards smaller Si-QD average diameter. When fitted with a stretched exponential the stretching factor is lower for samples with induced defects suggesting a larger distribution of lifetimes in these samples. The differences in results between samples indicate the need for further investigation. If as the PL spectra indicate, these induced vacancies result in increased PL intensity, a wider sample set should be prepared. Rather than implanting Si^+ as a technique for creating damage in SiO_2 layer a heavier element could be used to allow a wider set of samples. Taking into account all results found in this research it is possible to say that defect-mediated growth of Si-QD in SiO_2 is a topic that deserves further investigation.

7 Bibliography

Barbagiovanni, L.V. Goncharova, P.J. Simpson. "Electronic Structure Study of Si quantum dots in a SiO2 matrix: Analysis of Quantum Confinement Barriers." *Physical Review* 83 (2011): 1-6.

Canham, L.T. "Silicon quantum wire array fabrication by electrochemical and chemical dissolution of wafers." *Applied Physics Letters* 57 (1990): 1046.

Cy, Ng. "Performance of silicon nanocrystal non-volatile memory devices under various programming mechanisms." *Journal of Nanoscience and nanotechnology* 7 (2007): 329-334.

Dabrowski, Hans-Joachim Müssig. *Silicon Surfaces and Formation of Interfaces.* Singapore: Worl Scientific Publishing Co. Pte. Ltd, 2000.

Dippo, P. "Photoluminescence. Photonics Spectra." *NREL* 35 (2001): 73.

Dohnalova, K. "Time-resolved photoluminescence spectroscopy of the initial oxidation stage of small silicon nanocrystals." *Applied Physics Letters* 94 (2009): 3.

Garcia, G. "Size dependence of lifetime and absorption cross section of Si nanocrystals embedded in SiO2." *Applied Physics Letters* 82 (2003): 3.

Goncharova, L. *Interface Science Western Research.* July 22, 2013. http://www.isw.physics.uwo.ca/facilities/Tandetron/index.htm (accessed July 22, 2013).

Graydon, O. "A new Colour of optical chips." *Nature Photonics* 1 (2007): 298.

Gritsenko, V.A. "Silicon dots/clusters in silicon nitride: photoluminescence and electron spin resonance." *Thin Solid Films* 353 (1999): 20-24.

Hiller, Mihaela Jivanescu. "Pb(0) centers at the Si-nanocrystal/SiO2 interface as the dominant photoluminescence quenching defect." *Journal of Applied Physics* 107 (2010): 4.

Humphreys, C. J. "Solid State Lighting." *Material Research Society* 33 (2008): 459-470.

Iwayama, T. Shimizu. "Visible photoluminescence in Si+-implanted thermal oxide films on crystalline Si." *Appl. Phys. Lett.* 65 (1994): 1814.

Jayatilleka, C. R. Mokry, PJ. Simpson. "Probing energy transfer in an ensemble of silicon nanocrystals." *J. Appl. Phys.* 110 (2011): 1.

Kang, B. Arnold, C. J. Summers, B. K. Wagner. "Synthesis of Silicon Quantum Dots Buried SiOx Films with Controlled Luminescence Properties for Solid State Lighting." *Nanotechnology* 17 (2006): 4477-4482.

Kittler, M. "The Silicon Age." *physica status solidi* 203 (2006): 653.

Kovalev, D. "Breakdown of k-conservation rule in Si nanocrystals." *Phys Rev. Lett.* 81 (1998): 2803.

Kudo, Akihiko. "Luminescent Properties of Rare-Earth-Metal Ion-Doped KLaNb2O7 with Layered Perovskite Structures." *Chemistry of Materials* 9 (1997): 664-669.

Kuhn, Mark Y. Liu and Harold Kennel. *Technology Options for 22nm and Beyond.* Hillsboro: Intel Corporation, 2010.

Lee, Benjamin G. "Strained Interface Defects in Silicon Nanocrystals." *Advanced Functional Materials* 22 (2012): 3223-3232.

Liu, C.Y. "Optimization of Si NC/P3HT Hybrid Solar Cells." *Advanced Functional Materials* 20 (2010): 2157-2164.

M.Dovrat. "Radiative versus nonradiative decay processes in silicon nanocrystals probed by time-resolved photoluminescence spectroscopy." *Physical Review* 69 (2004): 1.

Mokry. "Role of vacancy-type defects in the formation of silicon nanocrystals." *Journal of Applied Physics* 105 (2009): 1-6.

Pacchioni, Linards Skuja, David L. Griscom. *Defects in SiO2 and Related Dielectrics: Science and Technology.* Springer, 2000.

Pankove, J.I. *Electroluminescence, Topics in Applied Physics.* Vol. 17. Springer, 1977.

Reimer, L. *Scanning Electron Microscopy: Physics of Image Formation and Microanalysis.* Springer, 1998.

Shimizu-Iwayama, Katsunori Fujita. "Visible photoluminescence in Si+-implanted silica glass." *J. Appl. Phys.* 65 (1994): 7779.

Streetman, Ben G. *Solid State Electronic Devices.* 2. Vol. 1. Prentice Hall, 1997.

Wilson, Peter Mascher. "Effect of thermal treatment on the growth, structure and luminescence of nitride-passivated silicon nanoclusters." *Nanoscale Research Letters* 6 (2011): 168.

Yu, D. P. "Direct evidence of quantum confinement from the size dependence of the photoluminescence." *Physical Review* 59 (1998): 1097-1098.

Zhao, Y. "Photonic crystals in Bioassays." *Advanced Functional Materials* 20 (2010): 2970-2988.

Zhizhong, Y. "Silicon Nanocrystals as an Enabling Material for Silicon Photonics." *Proceedings of IEEE* 97 (2009): 1250-1268.

Ziegler. *The Stopping and Range of Ions in Matter (SRIM).* 2013. www.srim.org (accessed April 10, 2013).

List of Abbreviations

Si-QD – Silicon Quantum Dot

SiO_2 – Silicon Dioxide

PL – Photoluminescence

TRPL – Time Resolved Photoluminescence

EPR – Electron Paramagnetic Spectroscopy

PMT – Photomultiplier Tube

LED – Light Emitting Diode
CB – Conduction Band
VB – Valence Band
c-Si – Crystalline silicon
IC – Integrated Circuit
SRIM – Stopping Range of Ions in Matter

Curriculum Vitae

Name:	John Phelan
Post-secondary Education and Degrees:	University of Western Ontario, London, Ontario. 2011 – 2013, MSc in Physics
Post-secondary Education and Degrees:	Dublin Institute of Technology, Dublin, Ireland. 2006 – 2010, BSc in Physics